Compact Er:Yb:glass-laser-based supercontinuum source for high-resolution optical coherence tomography

M. C. Stumpf,[1,*] S. C. Zeller,[1] A. Schlatter,[1] T. Okuno,[2] T. Südmeyer,[1] U. Keller[1]

[1]*Department of Physics, Institute of Quantum Electronics, ETH Zurich, 8093 Zurich, Switzerland*
[2]*Optical Communications R&D Laboratories, Sumitomo Electric Industries, Ltd., Japan*
[*]*Corresponding author: stumpf@phys.ethz.ch*

Abstract: We present a low coherence light source by direct supercontinuum generation from a diode-pumped, passively modelocked Er:Yb:glass-laser, which generates 198 fs transform-limited pulses with an average power of 100 mW at a repetition rate of 75 MHz. The pulse train is launched into a dispersion optimized highly nonlinear fiber for spectral broadening. The optical bandwidth spans from 1150 nm to 2400 nm, which is more than one octave. The potential for ultrahigh-resolution optical coherence tomography (OCT) is demonstrated by coherence measurements supporting an axial resolution of 3.5 µm in air.

OCIS codes: (170.4500) Optical coherence tomography; (320.7090) Ultrafast lasers; (170.3880) Medical and biological imaging; (060.7140) Ultrafast processes in fibers.

References and links

1. D. Huang, E. A. Swanson, C. P. Lin, J. S. Schuman, W. G. Stinson, W. Chang, M. R. Hee, T. Flotte, K. Gregory, C. A. Puliafito, and J. G. Fujimoto, "Optical coherence tomography," Science **254**, 1178-1181 (1991).
2. J. G. Fujimoto, "Optical coherence tomography for ultrahigh resolution in vivo imaging," Nat. Biotechnol. **21**, 1361-1367 (2003).
3. E. A. Swanson, J. A. Izatt, M. R. Hee, D. Huang, C. P. Lin, J. S. Schuman, C. A. Puliafito, and J. G. Fujimoto, "In-vivo retinal imaging by optical coherence tomography," Opt. Lett. **18**, 1864 (1993).
4. G. J. Tearney, M. E. Brezinski, B. E. Bouma, S. A. Boppart, C. Pitris, J. F. Southern, and J. G. Fujimoto, "In vivo endoscopic optical biopsy with optical coherence tomography," Science **276**, 2037-2039 (1997).
5. J. Welzel, E. Lankenau, R. Birngruber, and R. Engelhardt, "Optical coherence tomography of the human skin," Journal of the American Academy of Dermatology **37**, 958-963 (1997).
6. Y. Zhao, Z. Chen, C. Saxer, S. Xiang, J. F. de Boer, and J. S. Nelson, "Phase-resolved optical coherence tomography and optical Doppler tomography for imaging blood flow in human skin with fast scanning speed and high velocity sensitivity," Opt. Lett. **25**, 114-116 (2000).
7. M. E. Brezinski, G. J. Tearney, B. E. Bouma, J. A. Izatt, M. R. Hee, E. A. Swanson, J. F. Southern, and J. G. Fujimoto, "Optical Coherence Tomography for Optical Biopsy: Properties and Demonstration of Vascular Pathology," Circulation **93**, 1206-1213 (1996).
8. B. Colston, U. Sathyam, L. DaSilva, M. Everett, P. Stroeve, and L. Otis, "Dental OCT," Opt. Express **3**, 230-238 (1998).
9. J. A. Izatt, M. D. Kulkarni, S. Yazdanfar, J. K. Barton, and A. J. Welch, "In vivo bidirectional color Doppler flow imaging of picoliter blood volumes using optical coherence tomography," Opt. Lett. **22**, 1439-1441 (1997).
10. U. Morgner, W. Drexler, F. X. Kärtner, X. D. Li, C. Pitris, E. P. Ippen, and J. G. Fujimoto, "Spectroscopic optical coherence tomography," Opt. Lett. **25**, 111-113 (2000).
11. B. E. Bouma, L. E. Nelson, G. J. Tearney, D. J. Jones, M. E. Brezinski, and J. G. Fujimoto, "Optical Coherence Tomographic Imaging of Human Tissue at 1.55 µm and 1.81 µm Using Er- and TM-Doped Fiber Sources," J. Biomed. Opt. **3**, 76-79 (1998).
12. B. Bouma, G. J. Tearney, S. A. Boppart, M. R. Hee, M. E. Brezinski, and J. G. Fujimoto, "High-resolution optical coherence tomograhic imaging using a mode-locked Ti:Al2O3 laser source," Opt. Lett. **20**, 1486-1488 (1995).
13. W. Drexler, "Ultrahigh-resolution optical coherence tomography," J. Biomed. Opt. **9**, 47-74 (2004).
14. W. Drexler, U. Morgner, F. X. Kärtner, C. Pitris, S. A. Boppart, X. D. Li, E. P. Ippen, and J. G. Fujimoto, "In vivo ultrahigh-resolution optical coherence tomography," Opt. Lett. **24**, 1221-1223 (1999).

#94786 - $15.00 USD Received 8 Apr 2008; revised 27 Jun 2008; accepted 28 Jun 2008; published 1 Jul 2008

15. A. Kowalevicz, T. Ko, I. Hartl, J. Fujimoto, M. Pollnau, and R. Salathé, "Ultrahigh resolution optical coherence tomography using a superluminescent light source," Opt. Express **10**, 349-353 (2002).
16. Y. Wang, Y. Zhao, J. S. Nelson, Z. Chen, and R. S. Windeler, "Ultrahigh-resolution optical coherence tomography by broadband continuum generation from a photonic crystal fiber," Opt. Lett. **28**, 182-184 (2003).
17. http://www.superlumdiodes.com.
18. K. Bizheva, B. Považay, B. Hermann, H. Sattmann, W. Drexler, M. Mei, R. Holzwarth, T. Hoelzenbein, V. Wacheck, and H. Pehamberger, "Compact, broad-bandwidth fiber laser for sub-2-µm axial resolution optical coherence tomography in the 1300-nm wavelength region," Opt. Lett. **28**, 707-709 (2003).
19. I. Hartl, X. D. Li, C. Chudoba, R. K. Ghanta, T. H. Ko, J. G. Fujimoto, J. K. Ranka, and R. S. Windeler, "Ultrahigh-resolution optical coherence tomography using continuum generation in an air-silica microstructure optical fiber," Opt. Lett. **26**, 608-610 (2001).
20. N. Nishizawa, Y. Chen, P. Hsiung, E. P. Ippen, and J. G. Fujimoto, "Real-time, ultrahigh-resolution, optical coherence tomography with an all-fiber, femtosecond fiber laser continuum at 1.5 µm," Opt. Lett. **29**, 2846-2848 (2004).
21. U. Keller, D. A. B. Miller, G. D. Boyd, T. H. Chiu, J. F. Ferguson, and M. T. Asom, "Solid-state low-loss intracavity saturable absorber for Nd:YLF lasers: an antiresonant semiconductor Fabry-Perot saturable absorber," Opt. Lett. **17**, 505-507 (1992).
22. U. Keller, K. J. Weingarten, F. X. Kärtner, D. Kopf, B. Braun, I. D. Jung, R. Fluck, C. Hönninger, N. Matuschek, and J. Aus der Au, "Semiconductor saturable absorber mirrors (SESAMs) for femtosecond to nanosecond pulse generation in solid-state lasers," IEEE J. Sel. Top. Quantum Electron. **2**, 435-453 (1996).
23. G. J. Spühler, L. Krainer, E. Innerhofer, R. Paschotta, K. J. Weingarten, and U. Keller, "Soliton mode-locked Er:Yb:glass laser," Opt. Lett. **30**, 263-265 (2005).
24. F. X. Kärtner, I. D. Jung, and U. Keller, "Soliton Mode-Locking with Saturable Absorbers," IEEE J. Sel. Top. Quantum Electron. **2**, 540-556 (1996).
25. J. M. Dudley, G. Genty, and S. Coen, "Supercontinuum generation in photonic crystal fiber," Reviews of Modern Physics **78**, 1135-1184 (2006).
26. N. Nishizawa, and T. Goto, "Widely Broadened Super Continuum Generation Using Highly Nonlinear Dispersion Shifted Fibers and Femtosecond Fiber Laser," Jpn. J. Appl. Phys. **40**, 365-367 (2001).
27. N. Nishizawa, and J. Takayanagi, "Octave spanning high-quality supercontinuum generation in all-fiber system," J. Opt. Soc. Am. B **24**, 1786-1792 (2007).
28. J. W. Nicholson, R. Bise, J. Alonzo, T. Stockert, D. J. Trevor, E. Monberg, J. M. Fini, P. S. Westbrook, K. Feder, and L. Grüner-Nielsen, "Visible continuum generation using a femtosecond erbium-doped fiber laser and a silica nonlinear fiber," Opt. Lett. **33**, 28-30 (2008).
29. R. Paschotta, "Noise of mode-locked lasers. Part II: Timing jitter and other fluctuations," Appl. Phys. B **79**, 163-173 (2004).
30. A. Schlatter, B. Rudin, S. C. Zeller, R. Paschotta, G. J. Spühler, L. Krainer, N. Haverkamp, H. R. Telle, and U. Keller, "Nearly quantum-noise-limited timing jitter from miniature Er:Yb:glass lasers," Opt. Lett. **30**, 1536-1538 (2005).
31. T. Okuno, M. Onishi, T. Kashiwada, S. Ishikawa, and M. Nishimura, "Silica-Based functional fibers with enhanced nonlinearity and their applications," IEEE J. Sel. Top. Quantum Electron. **5**, 1385-1391 (1999).
32. J. Chen, J. W. Sickler, E. P. Ippen, and F. X. Kärtner, "High repetition rate, low jitter, low intensity noise, fundamentally mode-locked 167 fs soliton Er-fiber laser," Opt. Lett. **32**, 1566-1568 (2007).
33. K. L. Corwin, N. R. Newbury, J. M. Dudley, S. Coen, S. A. Diddams, B. R. Washburn, K. Weber, and R. S. Windeler, "Fundamental amplitude noise limitations to supercontinuum spectra generated in a microstructured fiber," Applied Physics B: Lasers and Optics **77**, 269-277 (2003).
34. N. R. Newbury, B. R. Washburn, K. L. Corwin, and R. S. Windeler, "Noise amplification during supercontinuum generation in microstructure fiber," Opt. Lett. **28**, 944-946 (2003).
35. A. Aguirre, N. Nishizawa, J. Fujimoto, W. Seitz, M. Lederer, and D. Kopf, "Continuum generation in a novel photonic crystal fiber for ultrahigh resolution optical coherence tomography at 800 nm and 1300 nm," Opt. Express **14**, 1145-1160 (2006).
36. S. Bourquin, A. Aguirre, I. Hartl, P. Hsiung, T. Ko, J. Fujimoto, T. Birks, W. Wadsworth, U. B¸nting, and D. Kopf, "Ultrahigh resolution real time OCT imaging using a compact femtosecond Nd:Glass laser and nonlinear fiber," Opt. Express **11**, 3290-3297 (2003).

1. Introduction

Optical coherence tomography (OCT) is an established method for cross-sectional imaging of biological tissue and materials [1]. It has been particularly successful for biomedical imaging, because high-resolution 2- and 3-dimensional images can be realized in a fast, non-invasive way. Currently, OCT is mostly used in ophthalmology [2, 3] but its medical impact has also been proven for gastroenterology [4], dermatology [5, 6], intra-arterial imaging [7] and dentistry [8]. In addition, recent developments also revealed the potential of OCT for imaging functional characteristics [6, 9, 10].

#94786 - $15.00 USD Received 8 Apr 2008; revised 27 Jun 2008; accepted 28 Jun 2008; published 1 Jul 2008

The key element of an OCT system is the employed light source, because it sets the principal resolution and penetration limits. The achievable resolution $1/\Delta z = (\pi\Delta\lambda) / 2(\ln 2)\lambda^2$ increases for larger bandwidth and decreases for larger center wavelength. The penetration depth is mainly determined by the absorption and scattering in the tissue, thus it depends on the wavelength of the light source and the sample material. For OCT in high-scattering materials, longer wavelengths are desirable, because they usually increase penetration depth due to a strong reduction of scattering [11]. However, a significantly larger optical bandwidth is required to achieve the same resolution.

Ti:Sapphire laser oscillators had a large influence on OCT development. These systems operate in the 800-nm region and achieve extremely broad bandwidth, resulting in highest resolutions of about 1 µm [12-16]. However, Ti:Sapphire oscillators can not be directly diode-pumped, and their complexity and cost is a challenge for commercial applications. Most clinical OCT-systems are currently based on superluminescent diodes, which are significantly cheaper and less complex. Superluminescent diodes are available in different spectral regions [17]; however, they still lack of equivalent bandwidth and do not support the same resolutions as the state-of-the-art solid-state laser systems. Diode-pumped solid-state lasers are an interesting alternative, combining ultrahigh-resolution and a compact, reliable and cost-effective setup. Different schemes have been investigated and resolutions up to 2 µm at 1.3 µm emission wavelength [18, 19] and up to 7.6 µm at 1.5 µm emission wavelength [20] have been demonstrated.

In this article, we present a compact and reliable source of low coherence light based on a passively modelocked femtosecond Er:Yb:glass laser operating at a wavelength of 1.5 µm. The laser output is directly launched into a dispersion-flattened, highly nonlinear fiber for supercontinuum generation. By coherence measurements we confirm an axial resolution of 3.5 µm in air, which is shorter than previously obtained in the 1.5-µm spectral region. In the following section, we give a detailed description of our femtosecond Er:Yb:glass oscillator. Subsequently, we address details of the supercontinuum generation. In the last section, the potential for OCT applications is evaluated by coherence measurements.

2. The femtosecond Er:Yb:glass oscillator

Passively modelocked femtosecond solid-state lasers based on the Er:Yb:glass gain material have a number of compelling advantages. They use standard telecom optical components and can be directly pumped by high-brightness, telecom grade laser diodes. Stable and self-starting modelocking can be achieved with a semiconductor saturable absorber mirror (SESAM) [21, 22]. We previously demonstrated an Er:Yb:glass laser generating 58 mW average power in 255-fs pulses [23]. The laser reported here is an improved version, which is more compact due to different dispersion compensation, generates shorter pulses and has higher output power.

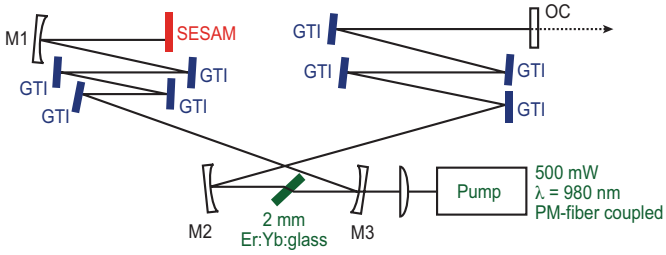

Fig. 1. Schematic of the laser cavity: SESAM, semiconductor saturable absorber mirror; M1 high reflectors at 1550 nm, radius of curvature 300 mm; GTI, high reflective GTI-mirror, dispersion -100 fs^2; M2, M3, high reflectors at 1550 nm, radius of curvature 75 mm; OC, output coupler, transmission 1.7 %.

Our setup (Fig. 1) consists of a standard delta-type cavity enabling soliton modelocking initiated by a SESAM [24]. For femtosecond pulse generation a low inversion level of the

#94786 - $15.00 USD Received 8 Apr 2008; revised 27 Jun 2008; accepted 28 Jun 2008; published 1 Jul 2008

active Erbium ions is required [23]. This is accomplished by long gain length (2 mm Er/QX phosphate glass with a doping concentration of $4.5 \cdot 10^{19}$ Er ions per cm^3 and $1.4 \cdot 10^{21}$ sensitizing Yb ions per cm^3), low intra-cavity loss and low output coupling (1.7%). The diffraction limited, fiber coupled diode delivers up to 500 mW pump light at 980 nm. The laser mode radius in the focus is only 28 µm in tangential and 20 µm in sagittal plane, respectively. This ensures sufficient self-phase modulation for soliton formation despite the relatively low glass nonlinearity ($n_2 \approx 3 \cdot 10^{-16}$ cm^2/W). The SESAM initiates and stabilizes the pulse formation. We employed a SESAM with a modulation depth of 0.5 %, a saturation fluence of 25 $\mu J/cm^2$, and linear losses below 0.2 %. For achieving soliton modelocking, we balance the intracavity self-phase modulation and negative group delay dispersion [24]. Our previous setup used a pair of fused-silica prisms for dispersion compensation [23], which has the advantage that the dispersion can be continuously optimized by changing the prism separation. In order to reduce losses and achieve a more stable and compact setup, we replaced the prims by dispersive mirrors. We used eight Gires-Tournois interferometer (GTI) type mirrors with a group delay dispersion (GDD) of -100 fs^2 each, corresponding to a total GDD of -1600 fs^2 per roundtrip. Higher compactness could be achieved by using a multipass configuration between two GTI-mirrors.

This laser produces stable soliton modelocking with up to 100 mW of average output power at a repetition rate of 75 MHz. The pulses had a duration of 198 fs and an optical bandwidth of 13.1 nm at FWHM (Fig. 2a,b). The corresponding time-bandwidth product of 0.321 exceeds the theoretical limit by only 2 %. The excellent agreement with the fitting function indicates the high pulse quality of this laser.

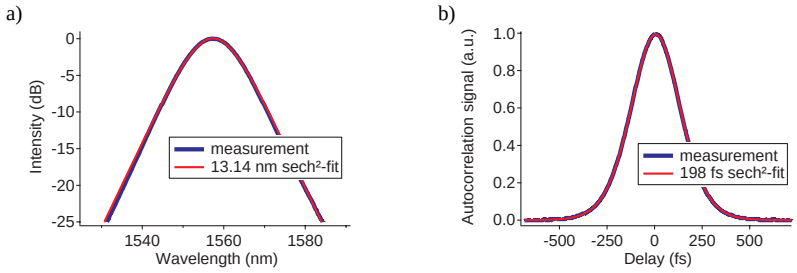

Fig. 2. Spectrum (a) and autocorrelation trace (b) of the generated pulses directly after the oscillator plotted with fits for a $sech^2$-pulse.

3. Supercontinuum generation

Supercontinuum generation by propagation of femtosecond pulses in a highly nonlinear fiber is an attractive method to provide a broad optical spectrum for OCT and other applications. The underlying physical mechanisms have been intensively studied and are well-understood [25-28]. In contrast to many other schemes based on diode-pumped femtosecond lasers, we generated the supercontinuum directly in a highly nonlinear fiber (HNLF) from the laser output without any additional pulse compression or pulse amplification stages (Fig. 3). This allows for a simple, compact and highly stable setup. The Er:Yb:glass laser runs at low saturated gain and low intracavity losses, resulting in lower quantum noise limit than for typical fiber or semiconductor lasers [29]. At higher repetition rates, lasers with equal gain characteristics have already proven a noise performance close to the quantum limit [30].

#94786 - $15.00 USD Received 8 Apr 2008; revised 27 Jun 2008; accepted 28 Jun 2008; published 1 Jul 2008

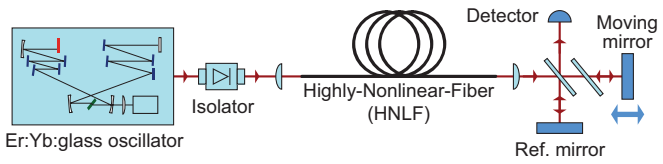

Fig. 3. Overview of the experimental scheme: The oscillator output is directly broadened by a highly nonlinear fiber (HNLF) and characterized by a Michelson Interferometer.

In order to generate a broad supercontinuum without any further amplification, we use a dispersion optimized HNLF manufactured by Sumitomo Electric Industries, Ltd. [31]. This fiber is realized in an all-solid design with a highly GeO_2-doped core surrounded by depressed cladding (Fig. 4). Diameters of the core and depressed cladding were optimized to provide a zero dispersion wavelength of 1535 nm and a flat dispersion profile around the pump wavelength (see red curve in Fig. 5, the dispersion slope is 0.02 ps/nm^2/km at 1.55 µm). The highly GeO_2-doped core and the small effective area of only 9.2 µm^2 result in a high nonlinear coefficient of 25 W^{-1}km^{-1}. This permits to generate an extremely broad spectrum at pulse durations above 200 fs and moderate pulse energies below 1 nJ.

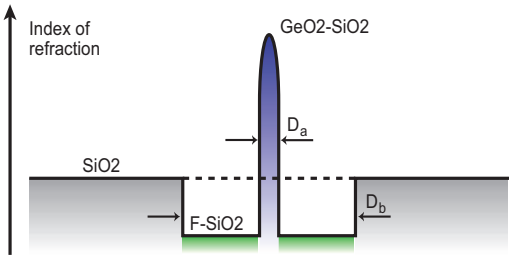

Fig. 4. Index of refraction profile of the highly nonlinear fiber (HNLF). The dispersion profile was adopted by the diameter D_a of the highly doped core and the diameter D_b of the depressed cladding.

The optical spectrum was measured with a commercially available monochromator (Spectral Products), which is optimized for operation in the infrared and far-infrared spectral region. For detection, an extended InGaAs photodiode with a sensitivity range up to more than 2.4 µm was employed. A polarization dependent calibration of the monochromator and the detector was performed with a white light source. The output pulses after the fiber were nearly unpolarized, and only minor differences between spectra of the horizontal and vertical polarization were observed. Fig. 5 shows the recorded spectrum of a 10- and a 5-meter long fiber piece at p-polarization. An additional 1-meter long piece of regular single mode fiber with a standard FC-connector was spliced to the end of the 10-meter HNLF for more convenient handling of the output.

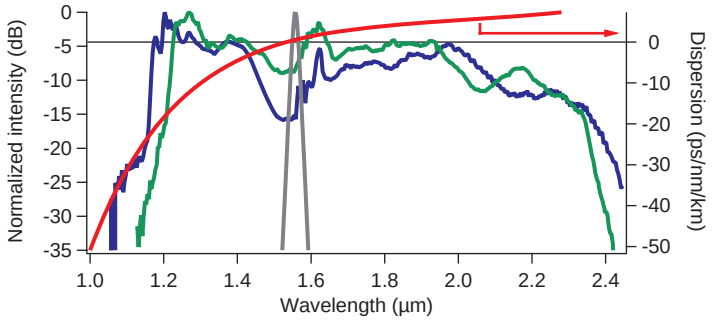

Fig. 5. Generated supercontinua. Blue line: spectrum of the 10-meter fiber; green line: spectrum of the 5-meter fiber; grey line: unbroaded laser spectrum; red line: dispersion profile of the HNLF.

#94786 - $15.00 USD Received 8 Apr 2008; revised 27 Jun 2008; accepted 28 Jun 2008; published 1 Jul 2008

In case of the 10-m long fiber, the HNLF generated a spectrum ranging over more than one optical octave from 1150 nm up to 2400 nm (at -20 dB level). More than 50 mW average power was measured at the output for an incident power of 100 mW. Using the 5-m long fiber and slightly increased pulse duration resulted in improved flatness of the generated spectrum (green curve in Fig. 5). In soliton modelocking, the pulse duration can easily be increased by providing larger GDD or lower pulse energy. For reasons of simplicity, we only reduced the pump power, resulting in nearly transform-limited 338-fs pulses with 61 mW average power. We obtained 31 mW supercontinuum with slightly reduced bandwidth, but improved flatness. These results are in agreement with the discussion presented in [26].

In order to evaluate the stability of our source we performed noise measurements. Noise characteristics are important indicators of the underlying physics and crucial for applications relying on stable signals. In particular, excess amplitude noise can reduce the high sensitivity commonly achieved by OCT systems. Usually, amplitude noise is quantified as relative intensity noise (RIN), which is often measured by monitoring the current of a photodiode directly on a microwave spectrum analyzer. This measurement technique, however, does not provide sufficient sensitivity to detect the very low noise levels of our laser. Therefore, we used a different method, which measures the RIN around zero frequency in the time domain. The AC-part of the photocurrent of this measurement was amplified, digitized, Fourier-transformed and normalized to the DC-power. Great care was taken to verify that the absolute noise level is determined correctly and that no distortion of the noise curves was caused by the transfer functions of the utilized electronics. This measurement near baseband is sensitive only to amplitude noise and is not affected by timing jitter. Fig. 6 shows the measured RIN of the oscillator, of the supercontinuum generated with the 10-m and the 5-m long fiber and the measurement system noise floor.

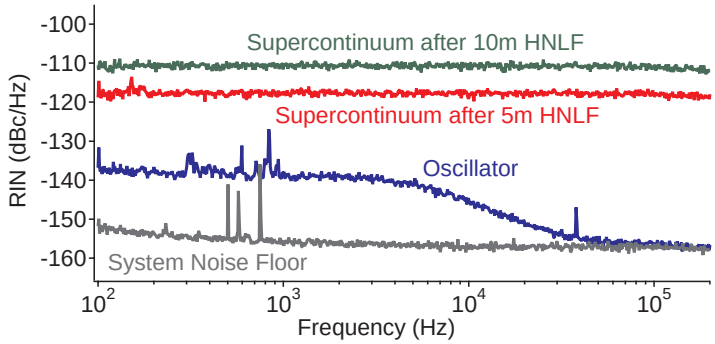

Fig. 6. Measured relative intensity noise (RIN). Blue line: RIN of the oscillator; green line: RIN of the supercontinuum generated with 10 m HNLF, red line: RIN of the supercontinuum generated with 5 m HNLF, grey line: RIN of the measurement system noise floor.

The cut-off frequency of the transimpedance amplifier gives an upper limit of the measurable frequency range. Within this range our laser has extremely low RIN better for example than reported by Chen at al. [32]. The peaks below 1 kHz are probably of technical origin, and have been largely reduced by replacing a standard laser diode driver with a low noise one. As the measurement confirms, supercontinuum generation gives rise to excess amplitude noise. In the literature different reasons for this behavior have been pointed out [33, 34]. Among the most important is amplification of input shot noise as well as spontaneous Raman emission during the supercontinuum generation itself. These effects also explain the white noise characteristics of the supercontinuum. As expected the excess noise of the longer fiber is higher due to its stronger nonlinear effects. Despite the increase of RIN during supercontinuum generation, the absolute level of the supercontinuum noise is still low. Although better noise performance has been achieved with a different supercontinuum

#94786 - $15.00 USD Received 8 Apr 2008; revised 27 Jun 2008; accepted 28 Jun 2008; published 1 Jul 2008

generation scheme [27], high sensitive OCT imaging has also been demonstrated at comparable noise levels [20, 35, 36]. Typically, OCT imaging does not exceed sensitivity levels of 110 dB [13], so it can be expected that the excess supercontinuum noise does not compromise OCT imaging sensitivity. In addition, OCT imaging is often performed with balanced detection, which strongly suppresses input noise.

4. Demonstrating OCT resolution

The extremely broad optical spectrum supports OCT imaging at high axial resolution. The coherence length was measured with a Michelson Interferometer, which was optimized for low chromatic aberration and a minimal dispersion difference between both interferometer arms. We used a Cr-Ni coating on a 100 µm thin fused silica substrate as beam splitter and compensated the material dispersion in the second arm with another 100 µm thin fused silica plate. With the spectra shown in Fig. 5, we measured the interferograms depicted in Fig. 7.

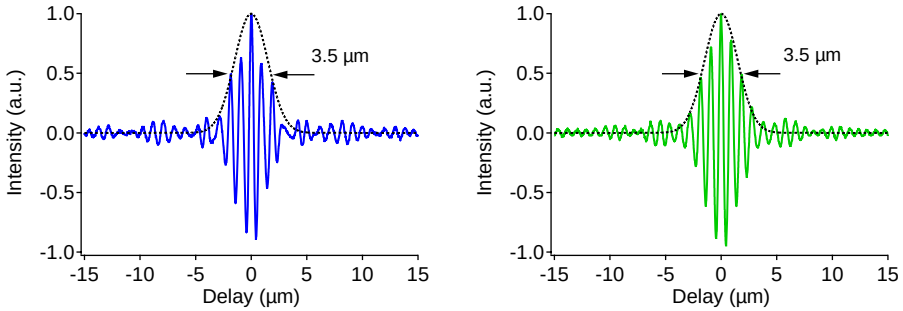

Fig. 7. Measured interferograms of the 10-meter (blue) and the 5-meter HNLF (green). The coherence length supports an axial resolution of 3.5 µm in air.

The recorded interferograms demonstrate the power for ultrahigh-resolution OCT. A coherence length of 3.5 µm is determined from the FWHM of an exponential fit. This corresponds to a maximum obtainable resolution in biological tissue of about 2.5 µm, which is to our knowledge the highest resolution ever obtained in this wavelength region.

Taken the high bandwidth $\Delta\lambda \approx 1\mu m$ of the supercontinuum, one can estimate the principal limit of axial resolution to $\Delta z = 2(\ln 2)\lambda^2 / (\pi\Delta\lambda) \approx 1\mu m$. There are mainly two reasons why this limit was not reached experimentally. First, a smooth spectral profile with flat edges is required to obtain maximum resolution. For this reason a more flat spectrum would be desirable, which could be achieved for instance with absorptive filters [13]. Second, the interferometer must handle the full bandwidth without distortion. A comparison between the spectrum, which is retrieved from the interferogram by Fourier-Transform and the one measured with the monochromator clearly reveals, that some filtering by the interferometer takes place (Fig. 8). This is mainly due to the spectral response of the detector but also due to remaining chromatic aberrations of the transfer optics and the beam splitter. These aberrations may have prevented higher resolutions in case of the 5-meter HNLF, which was at the output not spliced to a standard fiber, because the numerical aperture was considerably larger. Customized optics would overcome these limitations making a further increase in resolution feasible.

#94786 - $15.00 USD Received 8 Apr 2008; revised 27 Jun 2008; accepted 28 Jun 2008; published 1 Jul 2008

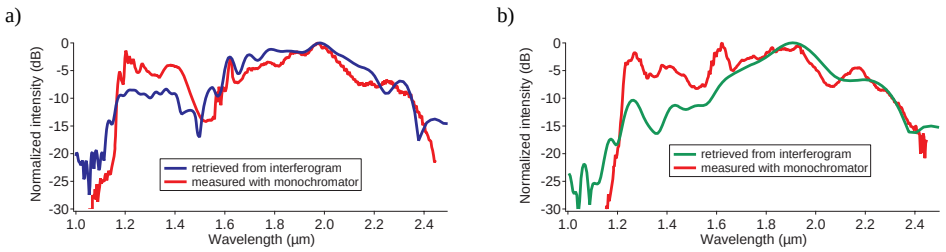

Fig. 8. Comparison between the spectrum retrieved from the interferogram and the spectrum measured with the monochromator (both curves include the response of the same detector) using (a) 10-meter HNLF and (b) 5-meter HNLF.

5. Conclusion

In conclusion, we have demonstrated a compact source suitable for ultrahigh resolution OCT operating in the 1.5-μm spectral region. This wavelength region is attractive for OCT applications, because in many types of biological tissues, optical backscattering is strongly reduced at longer wavelength, supporting a larger penetration depth [11]. The system is based on a compact, turn-key SESAM-modelocked Er:Yb:glass laser and spectral broadening in a highly nonlinear fiber. The Er:Yb:glass laser uses GTI-type mirrors for dispersion compensation and generates transform-limited 198-fs soliton pulses with an average output power of 100 mW. An octave-spanning supercontinuum was obtained from the dispersion-flattened, silica-based fiber. Due to the well-engineered fiber dispersion and nonlinearity, no pulse compression or pulse amplification before the supercontinuum generation is necessary, which would introduce additional noise. The coherence length of the supercontinuum was determined by a Michelson-Interferometer. We demonstrate a maximum obtainable resolution of about 3.5 μm in air, corresponding to about 2.5 μm in tissue, which is more than a factor of two better than previously achieved in the 1.5-μm wavelength regime.

Acknowledgment

This work was supported by the European Commission through CRAFT project MULTIWAVE (018074) and by ETH Research Grant TH-04 07-3.

#94786 - $15.00 USD Received 8 Apr 2008; revised 27 Jun 2008; accepted 28 Jun 2008; published 1 Jul 2008